Benefits of Inverted Fuel Geometry Implementation to Fast Reactor

Muhammad Farid Khandaq [a], Deokjung Lee [a*]
[a] *Department of Nuclear Engineering, Ulsan National Institute of Science and Technology (UNIST), 50 UNIST-gil, Eonyang-eup, Ulju-gun, Ulsan, 44919, Republic of Korea*
[*] *Corresponding author: deokjung@unist.ac.kr*

1. Introduction

The passive cooling system is considered essential for the advanced nuclear reactor, especially after the Fukushima accident, where the active cooling system failure caused a nuclear catastrophe. The performance of a passive cooling system is a function of resisting (e.g., core pressure drop) and driving forces (e.g., density difference and gravity). Accordingly, reducing the resisting force could increase the margin of coolant flow rate and enhance the passive cooling system. A potential approach to reduce the core pressure drop (ΔP) is using the inverted fuel geometry, where the coolant and fuel relative position is inverted compared to conventional pin-type fuel, as presented in Fig. 1. Implementing inverted fuel also potentially yields a lower maximum fuel temperature ($T_F^{\max}$) and higher fuel volume fraction (V_F).

This paper summarizes the improvement of inverted fuel implementation to a fast reactor. A direct comparison between conventional rod-type and inverted fuels is presented step-by-step from the fuel cell, fuel assembly, and reactor core.

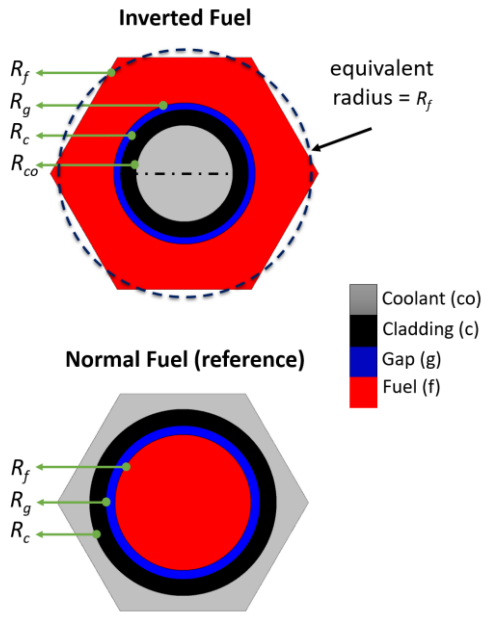

Fig. 1. Schematic of inverted and normal (reference) fuel cross-section.

2. Methods and Results

2.1 Reference Design (Conventional Pin-Rod Fuel)

The reference design of this study is MicroURANUS (MU) [1], an LBE fast reactor fueled with UO_2, generating 60 MW_{th} for 40 years without refueling and fuel shuffling, using conventional pin-type fuel. Table 1 summarizes the parameter of the MU fuel (pin) cell, where $\ddot{q}$ is volumetric power density, H is active core height, and v is coolant velocity.

Table I: Direct comparison of pin-type and inverted fuels.

Parameter	Unit	Pin-type (reference)	Inverted
Avg. $\ddot{q}$	W/cm^3	32.7	32.7
H	cm	155	155
$T_F^{\max}$	°C	547	545
T_F^{ave}	°C	473	515
v	m/s	0.94	0.93
V_F	%	**61.59**	**65.50** ↑
ΔP	kPa	**50.67**	**19.05** ↓
k_{inf}	-	**1.05552 ± 1.6E-4**	**1.07118 ± 1.7E-4**

2.2 Inverted Fuel Unit Cell

Coolant velocity (v), ΔP, $T_F^{\max}$, and V_F are used to compare the inverted and normal fuel performance. The coolant velocity and pressure drop for inverted fuel geometry are calculated using

$$v = \frac{\ddot{q}\, A_F\, H}{c_p \left(T_{co}^{out} - T_{co}^{in}\right) \rho\, A_{co}}, \quad (1)$$

$$\Delta P = \rho f \frac{H}{D_h} \frac{v^2}{2}, \quad (2)$$

where A_F and A_{co} are fuel and coolant area (also valid for normal fuel by adjusting the geometry variables). To

solve fuel temperature distribution as well as $T_F^{\max}$, an equivalent radius of hexagonal geometry is used, and solid-like in the gap is assumed — hence the steady state general heat conduction equation in cylindrical-coordinate can be employed,

$$\frac{1}{r}\frac{d}{dr} r\,k\frac{dT}{dr} + \ddot{q} = 0 . \quad (3)$$

The temperature distribution in the cladding is calculated as

$$T(R_{co} \le r \le R_c) = \frac{\dot{q}}{2\pi}\left[\frac{1}{k_c}\ln\left(\frac{r}{R_{co}}\right) + \frac{1}{h_{co}R_{co}}\right] + T_{co}, \quad (4)$$

for the gap

$$T(R_c \le r \le R_g) = \frac{\dot{q}}{2\pi}\frac{1}{k_g}\ln\left(\frac{r}{R_c}\right) + T_c, \quad (5)$$

and for the fuel

$$T(R_g \le r \le R_f) = \frac{\ddot{q}}{2\,k_f}\left[R_f^2\ln\left(\frac{r}{R_g}\right) + \frac{R_g^2 - r^2}{2}\right] + T_g, \quad (6)$$

where $\dot{q}$ is linear power density, k_x is corresponding thermal conductivity, h_{co} is coolant heat transfer coefficient, T_x is temperature evaluated at T_x, and $T(R_f) = T_F^{\max}$.

Using above equations, a multivariable diagram ($v, \Delta P, T_F^{\max} - D_{co}, V_F$) is constructed to incorporate inverted fuel performance in a single graph, as presented in Fig. 2, with $v, \Delta P, T_F^{\max}$ is parameterized by coolant channel diameter (D_{co}), and V_F. Each line on this graph represents a specific characteristic. For example, the v = 0.94 m/s line points that any geometry at this line has a coolant velocity of 0.94 m/s; however, with a different $\Delta P, T_F^{\max}$.

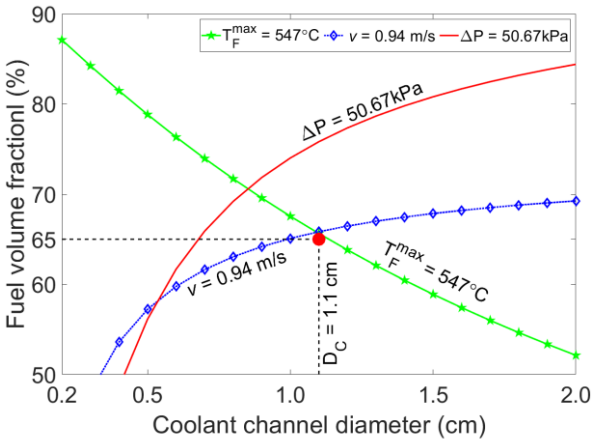

Fig. 2. Multivariable diagram ($v, \Delta P, T_F^{\max} - D_{co}, V_F$).

It should be noted that values on this graph are based on the normal fuel performance (see Table I), so a direct comparison between pin-type and inverted fuel can be performed. This diagram provides comprehensive information in a broader design space that allows the reactor designer to assess the fuel cell performance quickly.

A red dot in Fig.2 points to the location where the inverted and pin-type fuels have approximately the same v and $T_F^{\max}$. This shows that inverted fuel (as presented in Table 1) has: 1) lower ΔP by a factor of 2.5, indicating a potential to enhance the safety margin by providing extra coolant flow rate or to increase the reactor economy by decreasing pump power consumption to circulate the coolant; 2) about 3.9% higher V_F yields a better neutronic environment indicated by higher k_{inf}.

2.3 Fuel Assembly

The fuel assembly (FA) is constructed using the optimized fuel cell geometry. Each FA consists of full (19), half (12), and one-third (6) of inverted fuel geometries, as shown in Fig.3. Installing an FA duct separating each FA causes a considerable decrease in V_F; fortunately, the ΔP is still lower than pin-type FA, as shown in Table II.

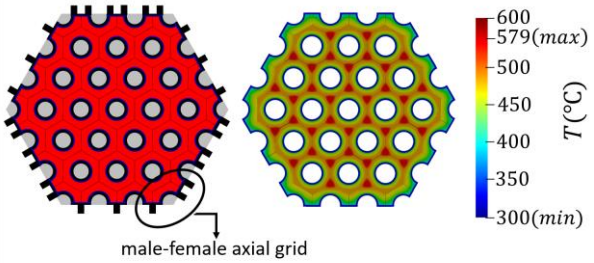

Fig. 3. Fuel assembly radial cross-section and fuel temperature distribution.

Table II: Comparison of FA of pin-type and inverted fuels.

Parameter	Unit	Pin-type FA	Inverted FA
V_F	%	**59.59**	**60.78** ↑
ΔP	kPa	**50.67**	**19.15** ↓
k_{inf}	-	1.04645 ± 1.7E-4	1.05276 ± 1.4E-4

2.4 Inverted Core Fast Reactor (IC-FR)

The described reactor design is named Inverted Core Fast Reactor (IC-FR). For clarity, the terminology of

inverted fuel refers to the fuel unit cell, while the inverted core is for the core level. There are three types of FA based on enrichment levels, as depicted in Fig.4, intended for power flattening in the axial and radial directions.

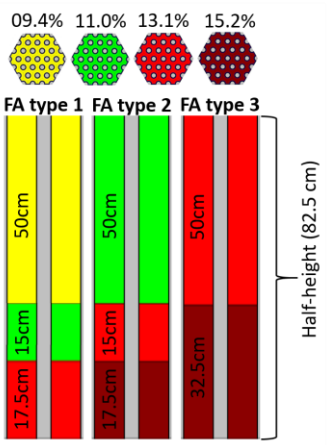

Fig. 4. IC-FR bottom-half FAs.

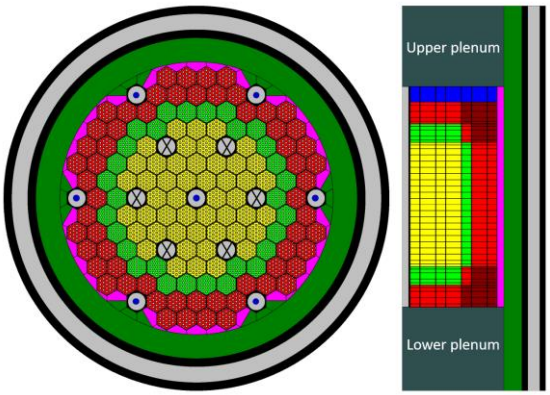

Fig. 5. IC-FR radial and axial cross-sections.

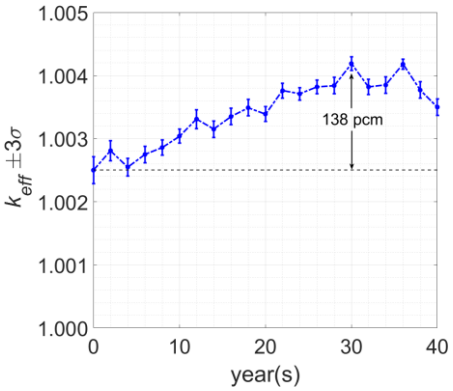

Fig. 6. IC-FR k_{eff} evolutions.

The radial and axial core cross-sections are presented in Fig.5. The core consists of 138 FAs, 7 regulating channels (Gd_2O_3), and 7 shutdown channels (B_4C). All the neutronic calculations were performed using Monte Carlo code MCS with ENDF/B-VII.1 library [2]. The core k_{eff} evolution, as shown in Fig.6, confirms the possibility of 40 years of operation without refueling and shuffling. It shows a small burnup reactivity swing of about 138 pcm (<< 1$) that IC-FR can be considered to have a flat reactivity swing over time.

The 3D power distributions at 0-year, 20-year, and 40-year are presented in Fig.7. At fresh condition, the core power is relatively flat (slightly more power at the core side), and it starts shifting to the core center due to the reduction of fissile inventory at the core side and ^{239}Pu buildup at the core center.

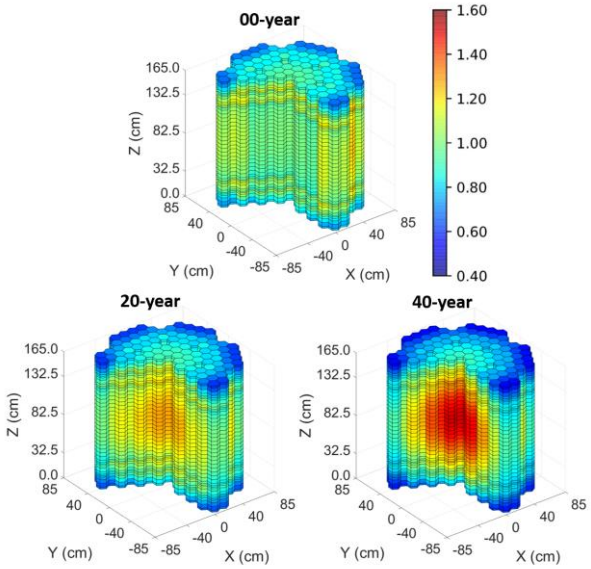

Fig. 7. IC-FR 3D power distribution at 0-year, 20-year, and 40-year operation.

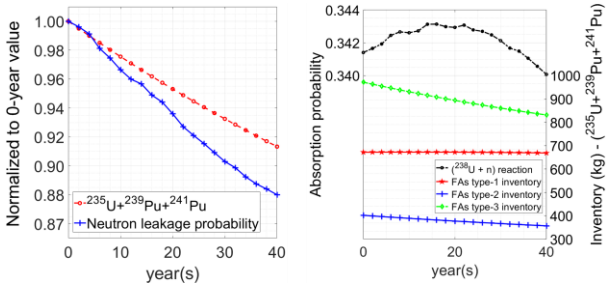

Fig. 8. (Right): reduction of core fissile inventory and neutron leakage; (Left): ^{238}U (*n, gamma*) reaction and FA-wise fissile inventory over time.

IC-FR is not a breeder reactor and has an average conversion ratio of 0.79. Despite a net depletion core, IC-FR can maintain its criticality by balancing the negative effect of fissile inventory reduction and the positive impact of the neutron leakage reduction as the power shifts to the core center, as presented on the left side of Fig.8 — all the values are normalized to the 0-year value. The ^{239}Pu production is not the same in every location; thus, fissile inventory varies in each FA

type, as shown on the right side of Fig.8. The ^{238}U (*n, gamma*) reaction (^{239}Pu build-up) accelerates at the early operation until it reaches its peak value at about 15 years due to power shifting to the core center where the lower enrichment is located and starts to decline as the ^{238}U concentration decreased owing to its (*n, gamma*) reaction and fast fission.

3. Conclusions

The multivariable diagram ($v, \Delta P, T_F^{\max} - D_{co}, V_F$) allows the reactor designer to perform an efficient inverted fuel cell optimization process by providing comprehensive thermal-hydraulic parameters in a single graph. The inverted fuel implementation to the fast reactor has at least two benefits: 1) higher volume fraction, which is advantageous for the neutronic aspect, and 2) lower core pressure drop that could enhance the reactor safety by providing an extra driving force for natural circulation, and increases system efficiency by lowering pump power consumption. To maintain k_{eff} for long life, the reduction of the neutron leakage as the power shift to the core center helps retain the neutron population inside the core that can compensate for the fissile inventory reduction over time.

Acknowledgment

This research was supported by the project (L20S089000) by Korea Hydro & Nuclear Power Co. Ltd and by the National Research Foundation of Korea (NRF) grant funded by the Korea government (MSIT). (No.NRF-2021M2D1A101906111).

REFERENCES

[1] Nguyen, T.D.C., Khandaq, M.F., Jeong, E., Choe, J., Lee, D., and Fynan, D.A., MicroURANUS: Core Design for Long-Cycle Lead-Bismuth-Cooled Fast Reactor for Marine Applications, Int. J Energy Res 45, 12426-12448, 2021.

[2] Lee, H.,Kim, W., Zhang, P., Lemaire, M., Khassenov, A., Yu, J., Jo, Y., Park, J., Lee, D., MCS — A Monte Carlo particle transport code for large-scale power reactor analysis, Annals of Nuclear Energy 139, 2020.